PHYSICAL REVIEW D **74,** 121503(R) (2006)

Merger of black hole-neutron star binaries: Nonspinning black hole case

Masaru Shibata[1] and Koji Uryū[2]

[1]*Graduate School of Arts and Sciences, University of Tokyo, Komaba, Meguro, Tokyo 153-8902, Japan*
[2]*Department of Physics, University of Wisconsin-Milwaukee, P.O. Box413, Milwaukee, Wisconsin 53201, USA*

(Received 11 October 2006; published 20 December 2006)

We perform a simulation for merger of a black hole (BH)-neutron star (NS) binary in full general relativity preparing a quasicircular state as initial condition. The BH is modeled by a moving puncture with no spin and the NS by the Γ-law equation of state with $\Gamma = 2$. Corotating velocity field is assumed for the NS. The mass of the BH and the rest-mass of the NS are chosen to be $\approx 3.2M_\odot$ and $\approx 1.4M_\odot$ with relatively large radius of the NS ≈ 14 km. The NS is tidally disrupted near the innermost stable orbit but $\sim 80\%$ of the material is swallowed into the BH with small disk mass $\sim 0.3M_\odot$ even for such small BH mass $\sim 3M_\odot$. The result indicates that the system of a BH and a massive disk of $\sim M_\odot$ is not formed from nonspinning BH-NS binaries, although a disk of mass $\sim 0.1M_\odot$ is a possible outcome.

DOI: 10.1103/PhysRevD.74.121503 PACS numbers: 04.25.Dm, 04.30.−w, 04.40.Dg

I. Introduction.— Merger of black hole (BH)-neutron star (NS) binaries is one of likely sources of kilometer size laserinterferometric gravitational wave detectors. Although such system has not been observed yet, statistical studies based on the stellar evolution synthesis suggest that the merger will happen more than 10% as frequently as the merger of binary NSs [1,2]. Thus, the detection of such system will be achieved by laserinterferometers in near future.

According to a study based on the tidal approximation (which is referred to as a study for configuration of a Newtonian star in circular orbits around a BH in its relativistic tidal field; e.g., [3–7]), the fate is classified into two cases, depending on the mass ratio $q \equiv M_{\rm NS}/M_{\rm BH}$, where $M_{\rm BH}$ and $M_{\rm NS}$ denote the masses of BH and NS, respectively. For $q \lesssim q_c$, the NS of radius R will be swallowed into the BH horizon without tidal disruption before the orbit reaches the innermost stable circular orbit (ISCO) [5,6], while for $q \gtrsim q_c$, NS may be tidally disrupted before plunging into BH. Here, the critical value of q_c depends on the BH spin and equation of state (EOS) of NS, and for the nonspinning case with stiff EOSs, $q_c \approx 0.3$–$0.35(R/5M_{\rm NS})^{-3/2}$ [6]. (Throughout this paper, we adopt the geometrical units $c = G = 1$.)

The second case has been studied with great interest because of the following reasons. (i) Gravitational waves at tidal disruption will bring information about the NS radius since the tidal disruption limit depends sensitively on it [8]. The relation between the mass and the radius of NSs may be used for determining the EOS of high density matter [9]. (ii) Tidally disrupted NSs may form a massive disk of mass ~ 0.1–$1M_\odot$ around the BH if the tidal disruption occurs outside the ISCO. Systems consisting of a BH and a massive, hot disk have been proposed as one of likely sources for the central engine of gamma-ray bursts (GRBs) with a short duration [10], and hence, merger of low-mass BH and NS is a candidate.

However, the scenario based on the tidal approximation studies may be incorrect since gravitational radiation reaction and gravitational effects of NS to the orbital motion are ignored. Radiation reaction shortens the time available for tidally disrupting NSs. The gravity of NS could increase the orbital radius of the ISCO and hence the critical value of the tidal disruption, q_c, may be larger in reality. Miller [11] estimates these ignored effects and suggests that NSs of canonical mass and radius will be swallowed into BH without tidal disruption. Moreover, NSs are described by the Newtonian gravity in the tidal approximation. If we treat it in general relativity, the gravity is stronger and hence tidal disruption is less likely.

Tidal disruption of NSs by a BH has been investigated in the Newtonian [12] and approximately general relativistic (GR) simulation [7,13]. However, a simulation in full general relativity is required (see [14] for an effort). In this paper, we present our first results for fully GR simulation, performed by our new code which has been improved from previous one [15,16]; we enable to handle orbiting BHs adopting the moving puncture method recently developed [17] (see also [18] for detailed calibration). As the initial condition, we prepare a quasicircular state computed in a new formalism described below. In this paper, we focus on whether NSs of realistic mass and radius is tidally disrupted to form a massive disk around nonspinning BHs. We will illustrate that a disk with mass $\sim M_\odot$ is an unlikely outcome for plausible values of NS mass and radius although a disk of mass of $O(0.1M_\odot)$ is possible.

II. Formalism for a quasicircular state.— Three groups have worked in computing quasicircular states of BH-NS binaries [19–21]. Here, we propose a new method for computing accurate quasicircular states that can be used for numerical simulation in the moving puncture framework [17].

Even just before the merger, it is acceptable to assume that BH-NS binaries are in a quasicircular orbit since the time scale of gravitational radiation reaction is a few times longer than the orbital period. Thus, we assume the presence of a helical Killing vector around the mass center of

the system, $\ell^\mu = (\partial_t)^\mu + \Omega(\partial_\varphi)^\mu$, where the orbital angular velocity Ω is constant.

Next, we assume that the NS is corotating around the mass center of the system. Irrotational velocity field is believed to be more realistic for BH-NS binaries [22] but we do not choose it in this paper. The NSs in corotation are more subject to tidal disruption than in irrotation (e.g., [4]) since the outer part has larger angular momentum than the inner part and thus outward mass ejection more easily occurs. If a corotating NS is stable against tidal disruption, this will be also the case for the irrotational NS of the same mass and radius.

The assumption of corotating velocity field in the helical symmetric spacetime yields the first integral of the Euler equation, $h^{-1}u^t = \text{const}$, where h is specific enthalpy defined by $1 + \varepsilon + P/\rho$, and ε, P, and ρ are specific internal energy, pressure, and rest-mass density, respectively. In the present work, we adopt the Γ-law EOS with $\Gamma = 2$; $P = \rho\varepsilon = \kappa\rho^2$ with κ an adiabatic constant. u^μ denotes the four velocity and u^t its time component. Assumption of corotation implies $u^\mu = u^t\ell^\mu$.

For a solution of geometric variables of quasicircular orbits, we adopt the conformal flatness formalism for three-geometry. In this formalism, the solution is obtained by solving Hamiltonian and momentum constraint equations, and an equation for the time slicing condition which is derived from $K_k{}^k = 0$ where K_{ij} is the extrinsic curvature and $K_k{}^k$ its trace [23]. Using the conformal factor ψ and the rescaled tracefree extrinsic curvature $\hat{A}_i{}^j = \psi^6 K_i{}^j$, these equations are, respectively, written

$$\Delta\psi = -2\pi\rho_{\rm H}\psi^5 - \frac{1}{8}\hat{A}_i{}^j\hat{A}_j{}^i\psi^{-7}, \tag{1}$$

$$\hat{A}_i{}^j{}_{,j} = 8\pi J_i\psi^6, \tag{2}$$

$$\Delta\Phi = 2\pi\Phi\left[\psi^4(\rho_{\rm H} + 2S) + \frac{7}{16\pi}\psi^{-8}\hat{A}_i{}^j\hat{A}_j{}^i\right], \tag{3}$$

where Δ denotes the flat Laplacian, $\rho_{\rm H} = \rho h(\alpha u^t)^2 - P$, $J_i = \rho h u_i$ and $S = \rho h[(\alpha u^t)^2 - 1] + 3P$. Here, α is the lapse function and Φ is defined by $\Phi \equiv \alpha\psi$.

We solve these equations in the framework of the puncture BH [17,24,25]. Assuming that the puncture is located at $\boldsymbol{r}_{\rm P}$, we set ψ and Φ

$$\psi = 1 + \frac{M_{\rm P}}{2r_{\rm BH}} + \phi \quad \text{and} \quad \Phi = 1 - \frac{C}{r_{\rm BH}} + \eta, \tag{4}$$

where $M_{\rm P}$ and C are positive constants, and $r_{\rm BH} = |x^k_{\rm BH}|$ ($x^k_{\rm BH} = x^k - x^k_{\rm P}$). Then elliptic equations for ϕ and η are derived. The constant $M_{\rm P}$ is arbitrarily given, while C is determined from the virial relation (e.g., [26])

$$\oint_{r\to\infty}\partial_i\Phi dS^i = -\oint_{r\to\infty}\partial_i\psi dS^i = 2\pi M, \tag{5}$$

where M is the ADM mass. The mass center is determined from the condition that the dipole part of ψ at spatial infinity is zero.

Equation (2) is rewritten setting

$$\hat{A}_{ij}(= \hat{A}_i{}^k\delta_{jk}) = W_{i,j} + W_{j,i} - \frac{2}{3}\delta_{ij}\delta^{kl}W_{k,l} + K^{\rm P}_{ij}, \tag{6}$$

where $K^{\rm P}_{ij}$ denotes the weighted extrinsic curvature associated with linear momentum of a puncture BH;

$$K^{\rm P}_{ij} = \frac{3}{2r^2_{\rm BH}}(n_iP_j + n_jP_i + (n_in_j - \delta_{ij})P_kn_k). \tag{7}$$

Here, $n^k = n_k = x^k_{\rm BH}/r_{\rm BH}$. P_i denotes linear momentum of the BH, determined from the condition that the total linear momentum of system should be zero;

$$P_i = -\int J_i\psi^6 d^3x. \tag{8}$$

The RHS of Eq. (8) denotes the total linear momentum of the companion NS. Then, the total angular momentum of the system is derived from

$$J = \int J_\varphi\psi^6 d^3x + \epsilon_{zjk}r^j_{\rm P}\delta^{kl}P_l. \tag{9}$$

The elliptic equation for $W_i(= W^i)$ is

$$\Delta W_i + \frac{1}{3}\partial_i\partial_k W^k = 8\pi J_i\psi^6. \tag{10}$$

Denoting $W_i = 7B_i - (\chi_{,i} + B_{k,i}x^k)$ where χ and B_i are auxiliary functions [27], Eq. (10) is decomposed as

$$\Delta B_i = \pi J_i\psi^6, \qquad \Delta\chi = -\pi J_ix^i\psi^6. \tag{11}$$

Computing BH-NS binaries in a quasicircular orbit requires to determine the shift vector even in the puncture framework. This is because u_i has to be obtained [it is derived from $u_k = \delta_{ki}u^t\psi^4(v^i + \beta^i)$ where $v^i = \Omega\varphi^i$]. The relation between β^i and $\hat{A}_{ij}$ is written

$$\delta_{jk}\partial_i\beta^k + \delta_{ik}\partial_j\beta^k - \frac{2}{3}\delta_{ij}\partial_k\beta^k = \frac{2\alpha}{\psi^6}\hat{A}_{ij}. \tag{12}$$

Operating $\delta^{jl}\partial_l$, an elliptic equation is derived

$$\Delta\beta^i + \frac{1}{3}\delta^{ik}\partial_k\partial_j\beta^j = 2\partial_j(\alpha\psi^{-6})\hat{A}^{ij} + 16\pi\alpha J_j\delta^{ij}, \tag{13}$$

which is solved in the same manner as that for W_i.

We have computed several models of quasicircular states and found that the relation between Ω and J approximately agrees with the 3rd Post-Newtonian relation [28]. This makes us confirm that this approach is a fair way for preparing quasicircular states. We also found that in this method, the shift vector at $\boldsymbol{r} = \boldsymbol{r}_{\rm P}$ automatically satisfies the condition $\beta^\varphi = -\Omega$ within the error of a few %. This implies that the puncture is approximately guaranteed to be in a corotating orbit in the solution.

III. Numerical results for quasicircular states.— BH-NS binaries in quasicircular orbits have been computed for a wide variety of models with $q = M_*/M_{\rm BH} \approx 0.3$–$0.5$ where M_* denotes baryon rest-mass of the NS. In the present work, the compactness of spherical NSs with rest-mass M_* is chosen to be ≈ 0.14. In the Γ-law EOSs, the mass and radius of NS are rescaled by changing the value of κ: In the following we fix the unit by setting that

$M_* = 1.4M_\odot$. In this case, $R \approx 13.8$ km, the gravitational mass is $\approx 1.30M_\odot$, and $M_*/\kappa^{1/2} = 0.147$. According to theories for NSs based on realistic nuclear EOSs [29], the radius of NS of $M_{\rm NS} \approx 1.4M_\odot$ is 11–13 km. Thus the radius chosen here is slightly larger than that of realistic NSs and is more subject to tidal disruption.

In computation, we focus only on the orbit of slightly outside of ISCO. Table I shows the quantities for selected quasicircular states with $q \approx 0.4$; model A is that used for the following numerical simulation and model B is very close to the tidal disprution limit of approximately the same mass as that of model A, showing that the model A has an orbit slightly outside the tidal disruption limit.

The tidal approximation studies suggest that for $q \gtrsim q_* \equiv 0.35(R/5M_{\rm NS})^{-3/2}[(M_{\rm BH}\Omega)^{-1}/6^{3/2}]$, NSs with $\Gamma = 2$ could be tidally disrupted by a nonspinning BH [6]. Here, $\Omega = M_{\rm BH}^{-1}/6^{3/2}$ is the angular velocity of the ISCO around nonspinning BHs. For model B, $q_* \approx 0.32$, and hence, $q > q_*$. According to the tidal approximation studies [5,6], such NS should be unstable against tidal disruption. Nevertheless, such equilibrium exists, proving that the tidal disruption limit in the framework of the tidal approximation does not give correct answer. Our studies indicate that the critical value q_* is $\approx 0.43(R/5M_{\rm NS})^{-3/2} \times [(M_{\rm BH}\Omega)^{-1}/6^{3/2}]$; tidal disruption of NS is much less likely than in the prediction by the tidal approximation [5,6]. For the typical NS of radius $R \sim 5M_{\rm NS}$ and mass $M_{\rm NS} \sim 1.4M_\odot$, $M_{\rm BH} \lesssim 3.3M_\odot$ will be necessary for $(M_{\rm BH}\Omega)^{-2/3} \geq 6$; this implies that canonical NSs will not be tidally disrupted outside ISCO by most of nonspinning BHs of mass larger than $\sim 3M_\odot$. Tidal disruption occurs only for NSs of relatively large radius and only for orbits very close to ISCO.

IV. Simulation for merger.— Even if tidal disruption of an NS occurs near ISCO, a massive disk may be formed around BH. To investigate this possibility we perform a numerical simulation adopting model A.

For the simulation, we initially reset the lapse (i.e., Φ) since the relation $\alpha \geq 0$ should hold. In the present approach we give Φ at $t = 0$ by the following equation

$$\Phi = \eta + \frac{1 + 0.1X^4}{1 + \sum_{m=1}^{3} X^m + 1.1X^4}, \tag{14}$$

where $X = C/r_{\rm BH}$. Then, $\alpha = 0$ only at puncture and otherwise $\alpha > 0$. Furthermore, for $r_{\rm BH} > C$, the values of Φ quickly approch to those of the quasicircular states.

TABLE I. Parameters of quasicircular states. Mass parameter of puncture, mass of BH, rest-mass of NS, mass and radius of NS in isolation, total mass of the system, nondimension angular momentum parameter, orbital period in units of M, and compactness of the system defined by $C_o = (M\Omega)^{2/3}$. Mass of BH is computed from the area of the apparent horizon A as $(A/16\pi)^{1/2}$. Mass is shown in units of $M_\odot$.

	$M_{\rm P}$	$M_{\rm BH}$	M_*	$M_{0\rm NS}$	R (km)	M	J/M^2	P_0/M	C_o
A	3.13	3.21	1.40	1.30	13.8	4.47	0.729	119	0.141
B	3.13	3.21	1.40	1.30	13.8	4.47	0.720	110	0.150

The numerical code for hydrodynamics is the same as that for performing merger of NS-NS binaries (high-resolution central scheme) [16]. However, we change equations for α, β^i, and ψ, and numerical scheme of handling the transport terms of evolution equations for geometries. For α and β^i we solve

$$(\partial_t - \beta^i\partial_i)\ln\alpha = -2K_k{}^k, \tag{15}$$

$$\partial_t\beta^i = 0.75\tilde{\gamma}^{ij}(F_j + \Delta t\partial_t F_j), \tag{16}$$

where $\tilde{\gamma}_{ij}$ is the conformal three-metric and $F_i = \delta^{jk}\partial_j\tilde{\gamma}_{ik}$. Δt denotes the time step for the simulation and the second term in the RHS of Eq. (16) is introduced for stabilization. The equation for the conformal factor is also changed to

$$\partial_t\psi^{-6} - \partial_i(\psi^{-6}\beta^i) = (\alpha K_k{}^k - 2\partial_i\beta^i)\psi^{-6}, \tag{17}$$

since ψ diverges at the puncture [17].

In addition, we have improved numerical scheme for the transport term of geometric variables $(\partial_t - \beta^i\partial_i)Q$ where Q is one of the geometric variables: First, we rewrite this term to $\partial_t Q - \partial_i(Q\beta^i) + Q\partial_i\beta^i$ and then apply the same scheme as in computing the transport term of the hydrodynamic equations to the second term (3rd-order interpolation scheme [15]). We have found that for evolving punctures, such high-resolution scheme for the transport term in the geometric variables are crucial. This is probably because of the fact that near punctures, some of geoemetric variables steeply vary and so is the term $\beta^i\partial_i Q$. For other terms in the Einstein's equation, we use the 2nd-order finite differencing as in [15,16]. (Note that in the case of nonuniform grid, 4-point finite differencing is adopted for $Q_{,ii}$ since 3-point one is 1st-order.) After we performed most of runs, we repeated some of computations with a higher-order scheme as used in [17,18]. With such scheme, convergent results are obtained with a relatively large grid spacing. However, the results are qualitatively unchanged and the extrapolated results (which are obtained in the limit of zero grid spacing) are approximately identical.

We adopt the cell-centered Cartesian, (x, y, z), grid to avoid the situation that the location of punctures (which always stay in the $z = 0$ plane) coincides with the grid location. The equatorial plane symmetry is assumed; the grid size is $(2N, 2N, N)$ for x-y-z. Following [30], we adopt a nonuniform grid; in the present approach, a domain of $(2N_0, 2N_0, N_0)$ grid zone is covered with a uniform grid of the spacing Δx and outside the domain, the grid spacing is increased according to $\xi\tanh[(i - N_0)/\Delta i]\Delta x$ where i denotes the i-th grid point in each direction. N_0, Δi, and ξ are constants. $\Delta x/M_{\rm P}$ is chosen to be 1/8, 9/80, 1/10, 7/80, and 3/40. As shown in [17], such grid spacing can resolve moving punctures. For $(N, N_0, \Delta i, \xi, \Delta x/M_p)$, we choose (i) (160 105 30,4.5,1/8), (ii) (200, 105, 30, 4.5, 1/8), (iii) (200, 105, 30,5, 1/8), (iv) (220, 125, 30, 5, 9/80), (v) (220, 125, 30, 6, 1/10), (vi) (220, 140, 30, 7, 7/80), and (vii) (220, 150, 9, 3/40). For $\Delta x = M_{\rm P}/8$ and

$N = 160$, we chose other values of N_0 and Δi, and found that results depend weakly on them. The grid covers a cube of edge length $2L$: For (i)–(vii), $L/\lambda = 0.46$, 0.78, 0.83, 0.78, 0.78, 0.65, and 0.59, respectively, where λ is the wavelength of gravitational waves at $t = 0$.

For a test, we performed a simulation for merger of two nonspinning BHs adopting the same initial condition as used in [17]. We focused particularly on the merger time and found that it varies with improving grid resolution. By the extrapolation, a true merger time is estimated. It is found that our result is $\approx 19M$ and agrees with those of [17] (see [31] for our results). This indicates that our code can follow moving punctures as in [17].

Figure 1 shows evolution of contour curves for ρ and velocity vectors for v^i in the equatorial plane together with the location of apparent horizons at selected time slices for (vii). Because of gravitational radiation reaction, the orbital radius decreases and then the NS is elongated (2nd panel). Because of the elongation, the quadrupole moment of the NS is amplified and the attractive force between two objects is strengthen [32]. This effect accelerates an inward motion and, consequently, the NS starts plunging to the BH at $t \sim 90M$. Soon after this time, the NS is tidally disrupted; but the tidal disruption occurs near the ISCO and

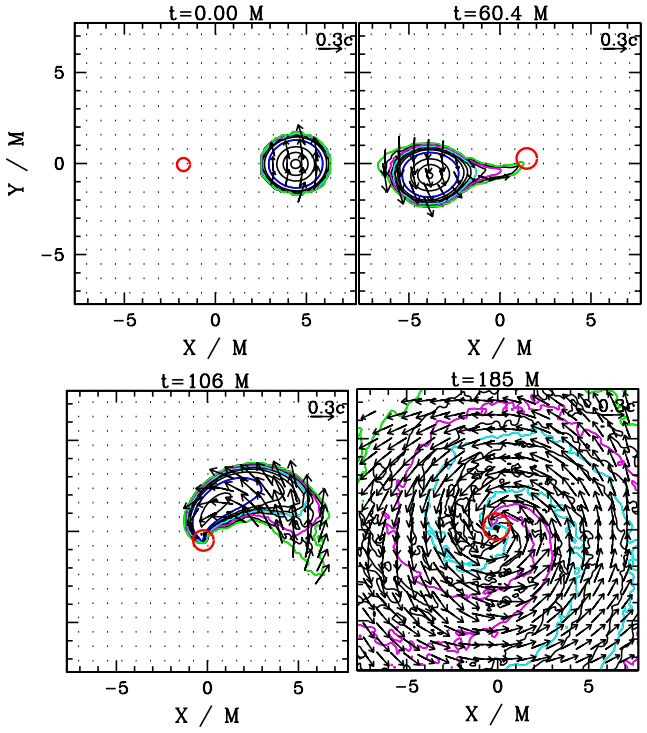

FIG. 1 (color online). Snapshots of the density contour curves for ρ in the equatorial plane for model A. The solid contour curves are drawn for $\rho = (1 + 2i) \times 10^{14}$ g/cm^3($i = 1, 2, 3$) and for $10^{14-0.5i}$ g/cm^3($i = 1 \sim 8$). The maximum density at $t = 0$ is $\approx 7.2 \times 10^{14}$ g/cm^3. (In the online version. the blue, cyan, magenta, and green curves denote 10^{14}, 10^{12}, 10^{11}, and 10^{10} g/cm^3, respectively.) Vectors indicate the velocity field (v^x, v^y), and the scale is shown in the upper right-hand corner. The thick (red) circles are apparent horizons.

hence the material in the inner part is quickly swallowed into the BH (3rd panel). On the other hand, because of the outward angular momentum transfer, the material in the outer part of the NS forms a disk with the maximum density $\sim 10^{12}$ g/cm^3 (4th panel).

However, mass of the disk is not large. Figure 2(a) shows evolution of baryon rest-mass located outside apparent horizons $M_{r>r_{\rm AH}}$. We find that $\sim$80% of the mass is swallowed into the BH in $t \sim 130M \sim 2$ ms, and swallowing continues after this time [33]. The value of $M_{r>r_{\rm AH}}$ depends systematically on Δx; we find that the results for (v)–(vii) at late times approximately obey a relation of convergence, i.e., $M_{r>r_{\rm AH}}(t) = a(t) + b(t)\Delta x^n$ where $a(t)$ and $b(t)$ are functions of time. The order of convergence, denoted by n, is between 1st and 2nd order (i.e., $1 < n < 2$). Least-square fitting gives $a(t)$ at $t = 180M$ as $\approx 0.19M_*$ if we set $n = 2$ and as $0.28M_*$ for $n = 1$ (see the solid circles in Fig. 2(a)). Thus, the true result should be between $0.19M_*$ and $0.28M_*$.

The adopted NS has corotating velocity field and furthermore its radius is larger than canonical values. In reality, the disk mass would be smaller than this value. Hence it is unlikely that a massive disk with $\sim M_\odot$ is formed after merger of nonspinning BH of mass $M > 3M_\odot$ and canonical NS of mass $\approx 1.4M_\odot$ and radius $\approx$ 11–13 km, although a disk of mass of $\sim$0.2–0.3$M_\odot$ may be formed for small BH mass and short GRBs of total energy $\sim 10^{49}$ ergs may be explained (e.g., [34]).

Figure 2(b) shows the evolution of averaged violation of the Hamiltonian constraint. For the average, rest-mass density is used as a weight (see [15]) and the integral is performed for the region outside apparent horizons. Figure 2(b) shows that the Hamiltonian constraint converges approximately at 2nd order. This result is consistent

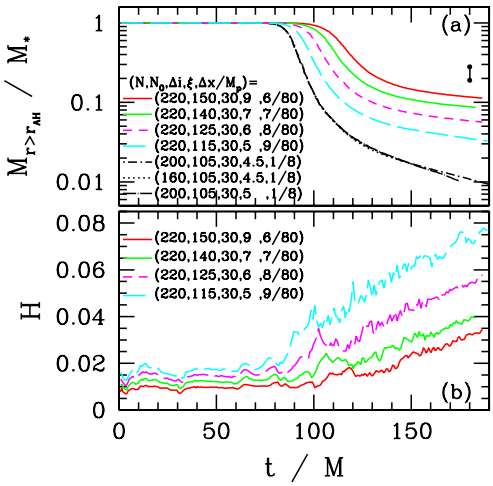

FIG. 2 (color online). (a) Evolution of baryon rest-mass located outside the apparent horizon for various grid settings. The plots for $\Delta x = M_{\rm P}/8$ almost coincide and show that the results depend weakly on the values of L and ξ. On the other hand, the results depend systematically on Δx (see text). (b) Evolution of averaged violation of Hamiltonian constraint for (iv)–(vii).

with the fact that the region except for the vicinity of BH is followed with 2nd-order accuracy.

To summarize, we have presented our first numerical results of fully GR simulation for merger of BH-NS binary, focusing on the case that the BH is not spinning initially and the mass ratio q is fairly large as 0.4. It is found that even with such high value of q, the NS is tidally disrupted only for the orbit very close to ISCO and 80–90% of the mass element is quickly swallowed into the BH without forming massive disks. The results do not agree quantitatively with the prediction by the tidal approximation study. The reasons are: (i) In the tidal approximation, one describes NSs by the Newtonian gravity. In general relativity, gravity is stronger and the tidal disruption is less likely. (ii) The time scale for angular momentum transfer during tidal disruption near the ISCO is nearly as long as the plunging time scale determined by gravitational radiation reaction and attractive force between two objects. Hence before the tidal disruption completes, most of the material is swallowed.

If the BH has a large spin, the final fate may be largely changed because of the presence of spin-orbit repulsive force. This force can weaken the attractive force between BH and NS and slow down the orbital velocity, resulting in smaller gravitational wave luminosity and longer radiation reaction time scale [35]. This effect may help massive disk formation. The study of spinning BH binaries is one of the next issues. The fate will also depend on EOS of NS [6] and mass of BH. Simulation with various EOSs and BH mass is also the next issue.

M. S. thanks Y. Sekiguchi for useful discussion. Numerical computations were performed on the FACOM-VPP5000 at ADAC at NAOJ and on the NEC-SX8 at YITP in Kyoto University. This work was supported in part by Monbukagakusho Grants (No. 17540232) and by NSF grants No. PHY0071044, 0503366.

[1] R. Narayan, B. Paczynski, and T. Piran, Astrophys. J. **395**, L83 (1992).
[2] R. Voss and T. M. Taulis, Mon. Not. R. Astron. Soc. **342**, 1169 (2003); K. Belczynski, T. Bulik, and B. Rudak, Astrophys. J. **571**, 394 (2002); V. Kalogera *et al.*, Astrophys. J. **601**, L179 (2004).
[3] L. G. Fishbone, Astrophys. J. **185**, 43 (1973); B. Mashhoon, Astrophys. J. **197**, 705 (1975); J.-A. Marck, Proc. R. Soc. A **385**, 431 (1983).
[4] M. Shibata, Prog. Theor. Phys. **96**, 917 (1996).
[5] P. Wiggins and D. Lai, Astrophys. J. **532**, 530 (2000).
[6] M. Ishii, M. Shibata, and Y. Mino, Phys. Rev. D **71**, 044017 (2005).
[7] J. A. Faber *et al.*, Phys. Rev. D **73**, 024012 (2006).
[8] M. Vallisneri, Phys. Rev. Lett. **84**, 3519 (2000).
[9] L. Lindblom, Astrophys. J. **398**, 569 (1992).
[10] C. L. Fryer, S. E. Woosley, M. Herant, and M. B. Davies, Astrophys. J. **520**, 650 (1999).
[11] M. C. Miller, Astrophys. J. **626**, L41 (2005).
[12] W. H. Lee and W. Kluzniak, Astrophys. J. **526**, 178 (1999); H. T. Janka, T. Eberl, M. Ruffert, and C. L. Fryer, Astrophys. J. **527**, L39 (1999); S. Rosswog, astro-ph/0505007.
[13] J. A. Faber, T. W. Baumgarte, S. L. Shapiro, and K. Taniguchi, Astrophys. J. **641**, L93 (2006).
[14] F. Löffler, L. Rezzolla, and M. Ansorg, Phys. Rev. D **74**, 104018 (2006).
[15] M. Shibata, K. Taniguchi, and K. Uryū, Phys. Rev. D **68**, 084020 (2003).
[16] M. Shibata, K. Taniguchi, and K. Uryū, Phys. Rev. D **71**, 084021 (2005); **73**, 064027 (2006).
[17] M. Campanelli, C. O. Lousto, P. Marronetti, and Y. Zlochower, Phys. Rev. Lett. **96**, 111101 (2006); J. G. Baker *et al.*, Phys. Rev. Lett. **96**, 111102 (2006).
[18] B. Brügmann *et al.*, gr-qc/0610128.
[19] M. Miller, gr-qc/0106017.
[20] K. Taniguchi, T. W. Baumgarte, J. A. Faber, and S. L. Shapiro, Phys. Rev. D **72**, 044008 (2005).
[21] P. Grandclement, Phys. Rev. D **74**, 124002 (2006) .
[22] C. S. Kochanek, Astrophys. J. **398**, 234 (1992); L. Bildsten and C. Cutler, Astrophys. J. **400**, 175 (1992).
[23] J. R. Wilson and G. J. Mathews, Phys. Rev. Lett. **75**, 4161 (1995).
[24] S. Brandt and B. Brügmann, Phys. Rev. Lett. **78**, 3606 (1997).
[25] M. D. Hannam, Phys. Rev. D **72**, 044025 (2005).
[26] E. Gourgoulhon, P. Grandclement, and S. Bonazzola, Phys. Rev. D **65**, 044020 (2002); G. Cook, Phys. Rev. D **65**, 084003 (2002).
[27] M. Shibata, Prog. Theor. Phys. **101**, 1199 (1999).
[28] L. Blanchet, Living Rev. Relativity **9**, 4 (2006).
[29] E. g., A. Akmal, V. R. Pandharipande, and D. G. Ravenhall, Phys. Rev. C **58**, 1804 (1998): F. Douchin and P. Haensel, Astron. Astrophys. **380**, 151 (2001).
[30] M. Shibata and T. Nakamura, Phys. Rev. D **52**, 5428 (1995).
[31] M. Shibata and K. Uryū, astro-ph/0611522 [Classical Quantum Gravity (to be published).
[32] D. Lai, F. A. Rasio, and S. L. Shapiro, Astrophys. J. Suppl. Ser. **88**, 205 (1993).
[33] $M_{r>r_{\rm AH}}$ is rest-mass of baryon located outside apparent horizons. Mass of disk located outside an ISCO around the formed BH is smaller than it. We follow the evolution of the rest-mass of baryon for $r > 3M$ and $r > 4.5M$ where $r = 3M$–$4.5M$ are approximate locations of the ISCO and find that their values are smaller than $M_{r>r_{\rm AH}}$ by $\sim$10% and 20%, respectively. Thus, the disk mass would be 0.8–$0.9M_{r>r_{\rm AH}}$ in reality.
[34] S. Setiawan, M. Ruffert, and H.-Th. Janka, Mon. Not. R. Astron. Soc. **352**, 753 (2004); W. H. Lee, E. R. Ruiz, and D. Page, Astrophys. J. **632**, 421 (2005).
[35] E.g., L. Kidder, C. M. Will, and A. G. Wiseman, Phys. Rev. D **47**, R4183 (1993).